HHS Public Access

Author manuscript

Proc SPIE Int Soc Opt Eng. Author manuscript; available in PMC 2017 November 21.

Published in final edited form as:

Proc SPIE Int Soc Opt Eng. 2016 March 29; 9788: . doi:10.1117/12.2216900.

Mutual Connectivity Analysis (MCA) Using Generalized Radial Basis Function Neural Networks for Nonlinear Functional Connectivity Network Recovery in Resting-State Functional MRI

Adora M. DSouza[1], **Anas Zainul Abidin**[2], **Mahesh B. Nagarajan**[3], and **Axel Wismüller**[1,2,3,4]

[1]Department of Electrical Engineering, University of Rochester, NY, USA

[2]Department of Biomedical Engineering, University of Rochester, NY, USA

[3]Department of Imaging Sciences, University of Rochester, NY, USA

[4]Faculty of Medicine and Institute of Clinical Radiology, Ludwig Maximilian University, Munich, Germany

Abstract

We investigate the applicability of a computational framework, called mutual connectivity analysis (MCA), for directed functional connectivity analysis in both synthetic and resting-state functional MRI data. This framework comprises of first evaluating non-linear cross-predictability between every pair of time series prior to recovering the underlying network structure using community detection algorithms. We obtain the non-linear cross-prediction score between time series using Generalized Radial Basis Functions (GRBF) neural networks. These cross-prediction scores characterize the underlying functionally connected networks within the resting brain, which can be extracted using non-metric clustering approaches, such as the Louvain method. We first test our approach on synthetic models with known directional influence and network structure. Our method is able to capture the directional relationships between time series (with an area under the ROC curve = 0.92 ± 0.037) as well as the underlying network structure (Rand index = 0.87 ± 0.063) with high accuracy. Furthermore, we test this method for network recovery on resting-state fMRI data, where results are compared to the motor cortex network recovered from a motor stimulation sequence, resulting in a strong agreement between the two (Dice coefficient = 0.45). We conclude that our MCA approach is effective in analyzing non-linear directed functional connectivity and in revealing underlying functional network structure in complex systems.

Keywords

Resting-state fMRI; functional connectivity; mutual connectivity analysis; convergent cross-mapping; non-metric clustering; Louvain method

[1] adora.dsouza@ur.rochester.edu; phone 603-729-7189; University of Rochester, NY.

1. INTRODUCTION

Over the past few decades, there has been significant growth in studies aimed at exploring connectivity in the human brain. To this end, various methods for analyzing functional MRI (fMRI) data, such as independent component analysis (ICA) [1] or seed-based functional connectivity analysis [2] have been developed. These approaches have certain drawbacks. For instance, seed-based approaches obtain a measure of connectivity for a few manually selected regions using linear cross-correlation analysis, which fails to capture non-linear information transfer between time series. ICA based methods do not obtain a directed connectivity score between every pair of voxel time courses in the brain. In this work, we use non-linear cross-prediction from one time series to another to obtain an influence score between them resulting in a non-linear, directed functional connectivity measure. These resulting scores are then used to recover the underlying network structure using non-metric clustering approaches. Previously, we investigated the use of local models to serve as time series predictors within this framework, discussed the conceptual relations of our approach to Convergent Cross-Mapping (CCM) [3], and demonstrated the applicability to fMRI data analysis [4]. Here, we demonstrate that this approach can be generalized to other non-linear predictors.

We use Generalized Radial Basis Functions (GRBF) neural networks as non-linear predictors used to establish the degree of dynamic coupling between two time series based on their cross-predictability. Subsequently, we use the information obtained based on the cross-predictability of the time series to recover the underlying network structure using non-metric clustering approaches, such as the Louvain method [5].

To quantitatively evaluate the performance of our approach, we test the ability of our method to quantify the influence a time series has on other time series and successfully recover network structure in a synthetic system model, where the ground truth is known by construction of the system. To evaluate the quality of recovered influence scores we calculate the Area Under the Receiver Operator Characteristic curve (AUC) against the known ground truth of the synthetic model. Agreement between the recovered network structure and the known network structure of the model is indicated by the Rand Index [6]. Here, we investigate the effect of training sequence time series length on the quality of network recovery.

We perform our analysis on resting-state fMRI data, which results in the recovery of a number of networks. We compare the recoverability of the motor-cortex network using resting-state data with the network recovered as a result of stimulating the motor cortex with a finger-tapping motor task stimulation experiment. The agreement between the two networks is quantified using the Dice Coefficient [7]. This work is embedded in our group’s endeavor to expedite ‘big data’ analysis in biomedical imaging by means of advanced machine learning and pattern recognition methods for computational radiology and radiomics, e.g. [8–32].

2. DATA

2.1 Synthetic model

We generated 50 synthetic models with 50 time series, each having 2000 temporal samples to investigate the efficacy of MCA to reliably estimate nonlinear influence scores and subsequently recover the modular structure of the network. The network was designed to have 5 distinct modules with a total number of 50 nodes as seen in Figure 1 with few interactions between modules.

Each module had 10 nodes with an intra-module node degree drawn from a normal distribution with mean 3 and standard deviation 1.2. The inter-module node degree was obtained from a half Gaussian distribution with mean 0 and standard deviation 1.2. The low inter-module connection density as compared to the intra-module connection density was chosen so as to define a clear module structure. Hence, the intra-module degree is much higher than the intermodule degree.

With this model we generated the 50-dimensional time series characterizing the system using p-th order Vector AutoRegressive (VAR) modelling:

$$\mathbf{x}(t) = \sum_{j=1}^{p} \mathbf{AR}_j g(\mathbf{x}(t-j)) + \mathbf{e}(t), t = p+1, \ldots, T,$$

where $\mathbf{x}(t) \in \mathbb{R}^{N \times 1}$, $\mathbf{x}(t) = (x_1(t), x_2(t), x_3(t), \ldots, x_N(t))^{\mathrm{T}}$ and N=50. $\mathbf{AR}_j \in \mathbb{R}^{N \times N}$ are the auto-regression (AR) model parameter matrices characterizing the influence of the nodes (time series) in the network on each other; for example, if node 'a' does not influence node 'b', $\mathbf{AR}_j(b, a) = 0\ \forall; j \in \{1,..., p\}$, where the order p=2, was used to generate the model. If node 'a' does influence node 'b', then $\mathbf{AR}_j(b, a) \neq 0$. The coefficients of $\mathbf{AR}_j(b, a)$ are chosen such that the generated time series are stationary. The time series $\mathbf{e}(t)$ was chosen as stationary uncorrelated Gaussian noise used in producing $\mathbf{x}(t)$. The quadratic transformation function g was applied to the time series (Fig. 1b). This was done to test the ability of our method to recover non-linear interactions in the system. The first 500 time points of the 50 generated time series were removed to ensure stability of the time series.

This model is similar to the model presented in [33] with the added non-linear transformation.

2.2 Functional MRI data

This study used scans acquired from a healthy male aged 26 years with a 1.5T GE SIGNA$^{\mathrm{TM}}$ (GE, Milwaukee, WI, USA) whole-body MRI scanner. Two sequences of images were obtained from two slice locations, which correspond to the motor cortex. One sequence was obtained under resting state conditions (resting-state sequence), where the subject was instructed to lie still with their eyes closed. The second sequence involved a finger-tapping task stimulus that activated the left motor cortex (LMC), the supplementary motor area (SMA) and the right motor cortex (RMC), which was used to localize the motor cortex areas in the subject (task sequence).

The scans were acquired with the following parameters: echo time (TE)– 40ms, echo repetition time (TR) – 0.5s and flip angle (FA) – 90°. 512 scans were acquired from the two slice locations, where each had a slice thickness of 10 mm and an in-plane resolution of 3.75 mm x 3.75 mm.

3. METHODS

3.1 Preprocessing

Before we analyzed the data, we performed a few pre-processing steps: 1) To compensate for motion artifacts, registration of the fMRI time series was performed. 2) Linear de-trending was performed to correct for signal drifts. 3) To eliminate initial saturation effects on the analysis, the first 24 scans were discarded. 4) The voxel time series were normalized to zero mean and unit standard deviation so as to focus on signal dynamics rather than amplitude [34].

3.2 MCA - Pair-wise affinity evaluation using Generalized Radial Basis Functions (GRBF) neural networks

We first build a pair-wise affinity matrix, **A**, generated by estimating the cross-predictability between every pair of voxel time courses in the brain. For example, consider two voxel time courses **X** and **Y** (where **X**, **Y** $\in \{\mathbf{X}_k, k = 1,...,n\}$).We obtain the matrix element $(\mathbf{A})_{\mathbf{X},\mathbf{Y}}$, which is a measure of the ability of **X** to predict **Y** and describes the degree of dynamic coupling between them.

To obtain $(\mathbf{A})_{\mathbf{X},\mathbf{Y}}$, we first break down **X**, of length l, into a set of vectors $\mathbf{x}_t$, $t \in \{1,2,...,l-d+1\}$ of dimension d, which can be interpreted as a sliding window of length d moving along **X**. The corresponding prediction target vectors for $\mathbf{x}_t$ are vectors $\mathbf{y}_t$ of dimension e. In this study, we chose $d = 20$ and $e = 1$, as we are interested in predicting one point in the future. The set of $\mathbf{x}_t$ and their corresponding $\mathbf{y}_t$ are split into training (Tr) and test (Te) sets. The cross-prediction between series is obtained using a Generalized Radial Basis Functions (GRBF) network with one hidden layer. The number of neurons in the hidden layer, k, correspond to the number of cluster centers in the d-dimensional space of the ($\mathbf{x}_t^{\mathrm{Tr}}$) vectors. We use k-means clustering to obtain the centers. The similarity of every vector ($\mathbf{x}_t^{\mathrm{Tr}}$) with every cluster center is obtained using a soft-max normalized Gaussian function, which defines the activations of the hidden layer neurons. Training of the output weights is done by minimizing the mean squared error between the estimated target point $\hat{\mathbf{y}}_t^{\mathrm{Tr}} = \boldsymbol{f}(\mathbf{x}_t^{\mathrm{Tr}})$ and the actual point $\mathbf{y}_t^{\mathrm{Tr}}$, where $\boldsymbol{f}$ is the non-linear mapping obtained using the trained GRBF neural network.

After concatenating the estimates $\hat{\mathbf{y}}_t^{\mathrm{Te}}$ to reconstruct $\hat{\mathbf{Y}}$, the affinity matrix element $(\mathbf{A})_{\boldsymbol{X},\boldsymbol{Y}}$ is computed as the Pearson's correlation coefficient between the prediction $\hat{\mathbf{Y}}$ and the actual time series **Y**. For more details on GRBF neural network training in this context, see [35].

3.3 MCA - Non-metric clustering: Louvain method

The affinity matrix **A** contains information about the causal influence of the time series on each other. We can use this information to extract functionally connected regions within the brain. To this end, we perform community detection using the Louvain method [5]. Louvain method extracts the underlying network structure by finding high modularity clusters in the network, where modularity is a measure of the strength of the intra-module links as compared to the intermodules links, thus, decomposing the complex network into clusters (or modules) with weak inter-module links and strong intra-module connections.

Modularity is given by:

$$Q=\frac{1}{2m}\sum_{i,j}\left[(\mathbf{A})_{\mathbf{i,j}}-\frac{k_i k_j}{2m}\right]\delta\left(C_i,C_j\right)$$

where $(\mathbf{A})_{\mathbf{i,j}}$ is the weight that represents the influence score from nodes *i* to *j*, $k_i = \Sigma_j(\mathbf{A})_{\mathbf{i,j}}$ is called the strength of connections to node *i*, *i* belongs to community C_i, $\delta(a,b) = 1$ when $a = b$, and 0 otherwise, and $m=\frac{1}{2}\sum_{ij}(\mathbf{A})_{\mathbf{i,j}}$ The modularity is optimized by an iterative process as proposed in [5]. This approach merges different nodes of the network into larger communities (modules) if the change in modularity is positive. The merging terminates when further addition of nodes to communities decreases the modularity of the network.

All procedures were implemented using MATLAB 8.1 (MathWorks Inc., Natick, MA, 2013). The Louvain method implementation was taken from [36].

4. RESULTS

4.1 Synthetic model

We tested the ability of the GRBF neural network to obtain causal influence scores for the synthetic models generated, where the ground truth of the actual time series connectivity is known by construction. Subsequently, network recovery was performed using the Louvain method. We used varying time series lengths of the data as a training set and tested the network for time series length of 1000. Network recovery accuracy using MCA was quantitatively evaluated by Receiver Operating Characteristic (ROC) analysis, where the Area Under the Curve (AUC) results and the Rand index [6] values achieved by the Louvain method are shown in table 1. The Rand index was calculated based on the fact that the 50 time series formed 5 sub-network modules with 10 time series each.

4.2 Network recovery in fMRI data

Results of network recovery of motor cortex from a single resting state fMRI slice through non-metric clustering of the affinity matrix using our MCA framework are shown in Figure 2. With Louvain method, we were able to recover the LMC, SMA and RMC as one module which demonstrates the applicability of our MCA approach to recover functionally connected networks in resting state fMRI data. Figure 2 shows a visual comparison between the recovered network and the localization aid defined by a finger-tapping motor-stimulation task fMRI experiment. The comparison between both yields a Dice coefficient of 0.45.

5. NEW AND BREAKTHROUGH WORK

We demonstrate the effectiveness of Mutual Connectivity Analysis (MCA), a computational framework for analyzing directed functional connectivity from resting state fMRI data and recovering underlying network structure. Previously, [4] we studied the use of local models to serve as non-linear time series predictors within the MCA framework, discussed the conceptual relations of our approach to Convergent Cross-Mapping (CCM) [3], and demonstrated the applicability to fMRI data analysis [4]. Here, we demonstrate that this approach can be generalized to other non-linear predictors such as the GRBF neural network. The high AUC values for the synthetic model demonstrate the ability of our method to accurately recover the interdependence of time series within a complex, nonlinear system. In addition, our results, quantified by the Rand index values on the synthetic model and the Dice coefficient value on the resting-state fMRI data, suggest that such an analysis can reveal useful information about the underlying network structure. We conclude that our MCA approach can provide useful contributions to analyzing complex non-linear systems with potential applications in clinical neuroradiology.

6. CONCLUSION

We present an approach for obtaining influence scores between every pair of time series in complex systems by using a Mutual Connectivity Analysis (MCA) framework with GRBF neural networks as non-linear predictors, followed by extracting the underlying network structure through non-metric clustering approaches, such as the Louvain method. The strong agreement between the recovered motor cortex network and the localization aid demonstrates the applicability of our method to investigating functional connectivity in resting-state functional MRI data of the human brain.

This work is not being and has not been submitted for publication or presentation elsewhere.

Acknowledgments

This research was funded by the National Institutes of Health (NIH) Award R01-DA-034977. The content is solely the responsibility of the authors and does not necessarily represent the official views of the National Institute of Health. This work was conducted as a Practice Quality Improvement (PQI) project related to American Board of Radiology (ABR) Maintenance of Certificate (MOC) for Prof. Dr. Axel Wismüller. The authors would like to thank Prof. Dr. Dorothee Auer at the Institute of Neuroscience, University of Nottingham, UK, for her assistance with the fMRI data acquisition process. The authors would also like to thank Dr. Lutz Leistritz and Prof. Dr. Herbert Witte of Bernstein Group from Computational Neuroscience Jena, Institute of Medical Statistics, Computer Sciences, and Documentation, Jena University Hospital, Friedrich Schiller University Jena, Germany, Dr. Oliver Lange and Prof. Dr. Maximilian F. Reiser of the Institute of Clinical Radiology, Ludwig Maximilian University, Munich, Germany for their support.

References

1. Beckmann CF, DeLuca M, Devlin JT, Smith SM. Investigations into resting-state connectivity using independent component analysis. Philosophical Translations of the Royal Society B: Biological Sciences. 2005; 360:1001–1013.
2. Biswal B, Yetkin FZ, Haughton VM, Hyde JS. Functional connectivity in the motor cortex of resting human brain using echo-planar MRI. Magnetic Resonance in Medicine. 1995; 34:537–541. [PubMed: 8524021]

3. Sugihara G, May R, Ye H, Hsieh CH, Deyle ER, Fogarty M, Munch S. Detecting causality in complex ecosystems. Science. 2012; 338:496–500. [PubMed: 22997134]
4. Wismüller, A., Abidin, AZ., DSouza, AM., Wang, X., Hobbs, SK., Leistritz, L., Nagarajan, MB. SPIE Medical Imaging. International Society for Optics and Photonics; 2015. Nonlinear functional connectivity network recovery in the human brain with mutual connectivity analysis (MCA): convergent cross-mapping and non-metric clustering. (pp. 94170M-94170M)
5. Blondel VD, Guillame J-L, Lambiotte R, Lefebvre E. Fast unfolding of communities in large networks. Journal of Statistical Mechanics: Theory and Experiment. 2008:P10008.
6. Rand WM. Objective criteria for the evaluation of clustering methods. Journal of the American Statistical Association (American Statistical Association). 1971; 66(336):846–850.
7. Dice LR. Measures of the Amount of Ecologic Association Between Species. Ecology. 1945; 26(3): 297–302.
8. Hoole P, Wismuller A, Leinsinger G, Kroos C, Geumann A, Inoue M. Analysis of tongue configuration in multi-speaker, multi-volume MRI data. Proc 5th Semin Speech Prod Model Data CREST Work Model Speech Prod Mot Plan Articul Model. 2000:157–160.
9. Wismuller, A. PhD Thesis. Technical University of Munich, Department of Electrical and Computer Engineering; 2006. Exploratory Morphogenesis (XOM): a novel computational framework for self-organization.
10. Wismuller, A., Dersch, DR., Lipinski, B., Hahn, K., Auer, D. ICANN 98. Springer; London: 1998. A neural network approach to functional MRI pattern analysis—clustering of time-series by hierarchical vector quantization; p. 857-862.
11. Wismüller, A., Vietze, F., Dersch, DR., Behrends, J., Hahn, K., Ritter, H. Neurocomputing. Vol. 48. Elsevier; 2002. The deformable feature map-a novel neurocomputing algorithm for adaptive plasticity in pattern analysis; p. 107-139.
12. Behrends, J., Hoole, P., Leinsinger, GL., Tillmann, HG., Hahn, K., Reiser, M., Wismuller, A. Bildverarbeitung fur die Medizin 2003. Springer; Berlin, Heidelberg: 2003. A segmentation and analysis method for MRI data of the human vocal tract; p. 186-190.
13. Wismuller A, Dersch DR. Neural network computation in biomedical research: chances for conceptual cross-fertilization. Theory in Biosciences. 1997; 116(3):229–240.
14. Bunte K, Hammer B, Villmann T, Biehl M, Wismuller A. Exploratory Observation Machine (XOM) with Kullback-Leibler Divergence for Dimensionality Reduction and Visualization. ESANN. 2010; 10:87–92.
15. Wismuller, A., Vietze, F., Dersch, DR., Hahn, K., Ritter, H. ICANN 98. Springer; London: 1998. The deformable feature map—adaptive plasticity for function approximation; p. 123-128.
16. Wismuller, A. Advances in Self-Organizing Maps. Springer; Berlin Heidelberg: 2009. The exploration machine—a novel method for data visualization; p. 344-352.
17. Wismüller, A. Method, data processing device and computer program product for processing data. US Patent. 7,567,889. 2009.
18. Meyer-Base, A., Jancke, K., Wismuller, A., Foo, S., Martinetz, T. Eng Appl Artif Intell. Vol. 18. Elsevier; 2005. Medical image compression using topology-preserving neural networks; p. 383-392.
19. Huber, MB., Nagarajan, M., Leinsinger, G., Ray, LA., Wismuller, A. SPIE Med Imaging. Vol. 7624. International Society for Optics and Photonics; 2010. Classification of interstitial lung disease patterns with topological texture features; p. 762410
20. Wismuller A. The exploration machine: a novel method for analyzing high-dimensional data in computer-aided diagnosis. SPIE Med Imaging. 2009:72600G–72600G.
21. Bunte, K., Hammer, B., Villmann, T., Biehl, M., Wismuller, A. Neurocomputing. Vol. 74. Elsevier; 2011. Neighbor embedding XOM for dimension reduction and visualization; p. 1340-1350.
22. Wismuller, A. Advances in Self-Organizing Maps. Springer; Berlin Heidelberg: 2009. A computational framework for nonlinear dimensionality reduction and clustering; p. 334-343.
23. Huber, MB., Nagarajan, MB., Leinsinger, G., Eibel, R., Ray, LA., Wismuller, A. Med Phys. Vol. 38. American Association of Physicists in Medicine; 2011. Performance of topological texture features to classify fibrotic interstitial lung disease patterns; p. 2035-2044.

24. Wismuller A, Verleysen M, Aupetit M, Lee JA. Recent Advances in Nonlinear Dimensionality Reduction, Manifold and Topological Learning. ESANN. 2010
25. Wismüller, A., Meyer-Baese, A., Lange, O., Reiser, MF., Leinsinger, G. Med Imaging, IEEE Trans. Vol. 25. IEEE; 2006. Cluster analysis of dynamic cerebral contrast-enhanced perfusion MRI time-series; p. 62-73.
26. Otto TD, Meyer-Base A, Hurdal M, Sumners D, Auer D, Wismuller A. Model-free functional MRI analysis using cluster-based methods. AeroSense. 2003; 2003:17–24.
27. Varini, C., Nattkemper, TW., Degenhard, A., Wismuller, A. Breast MRI data analysis by LLE. Neural Networks, 2004. Proceedings. 2004 IEEE Int. Jt. Conf; 2004. p. 2449-2454.
28. Huber, MB., Lancianese, SL., Nagarajan, MB., Ikpot, IZ., Lerner, AL., Wismuller, A. Biomed Eng IEEE Trans. Vol. 58. IEEE; 2011. Prediction of biomechanical properties of trabecular bone in MR images with geometric features and support vector regression; p. 1820-1826.
29. Meyer-Base A, Pilyugin SS, Wismuller A. Stability analysis of a self-organizing neural network with feedforward and feedback dynamics. Neural Networks, 2004 Proceedings 2004 IEEE Int Jt Conf. 2004; 2:1505–1509.
30. Wismüller, A., Meyer-Base, A., Lange, O., Schlossbauer, T., Kallergi, M., Reiser, MF., Leinsinger, G. J Electron Imaging. Vol. 15. International Society for Optics and Photonics; 2006. Segmentation and classification of dynamic breast magnetic resonance image data. 13020-013020-13
31. Nagarajan, MB., Huber, MB., Schlossbauer, T., Leinsinger, G., Krol, A., Wismuller, A. Mach Vis Appl. Vol. 24. Springer; Berlin Heidelberg: 2013. Classification of small lesions in dynamic breast MRI: eliminating the need for precise lesion segmentation through spatio-temporal analysis of contrast enhancement; p. 1371-1381.
32. Nagarajan, MB., Huber, MB., Schlossbauer, T., Leinsinger, G., Krol, A., Wismuller, A. J Med Biol Eng. Vol. 33. NIH Public Access; 2013. Classification of Small Lesions in Breast MRI: Evaluating The Role of Dynamically Extracted Texture Features Through Feature Selection.
33. Wismüller, A., Nagarajan, MB., Witte, H., Pester, B., Leistritz, L. SPIE Medical Imaging. International Society for Optics and Photonics; 2014. Pair-wise clustering of large scale Granger causality index matrices for revealing communities; p. 90381R-90381R
34. Wismüller A, Lange O, Dersch DR, Leinsinger GL, Hahn K, Pütz B, Auer D. Cluster analysis of biomedical image time-series. International Journal of Computer Vision. 2002; 46:103–128.
35. Wismüller A, Wang X, DSouza AM, Nagarajan MB. A Framework for Exploring Non-Linear Functional Connectivity and Causality in the Human Brain: Mutual Connectivity Analysis (MCA) of Resting-State Functional MRI with Convergent Cross-Mapping and Non-Metric Clustering. 2014 arXiv preprint arXiv:1407.3809.
36. Scherrer, A. [Last accessed July 3, 2014] “Community Detection algorithm based on Louvain method” (Version 1.0) [software]. Available from http://perso.uclouvain.be/vincent.blondel/research/Community_BGLL_Matlab.zip

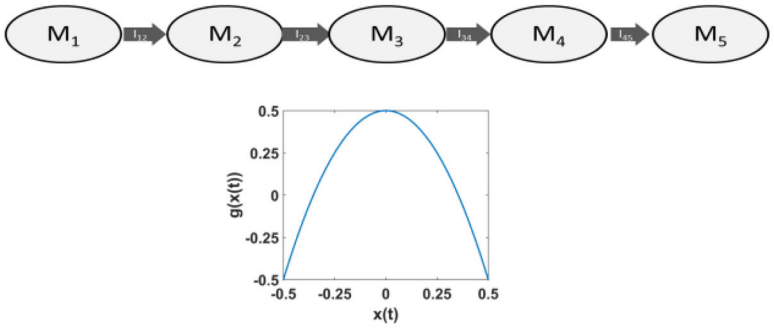

Figure 1.

(LEFT) Network with 5 modules M_1 to M_5. These modules have strong intra-module and weak inter-module connections, so as to have a network with modular structure, making feasible community detection using clustering approaches. I_{ab} (where, a ∈ {1..4} and b=a +1) represents the inter-module connections. (RIGHT) Transformation g, values above 0.5 and below −0.5 are mapped to 0.

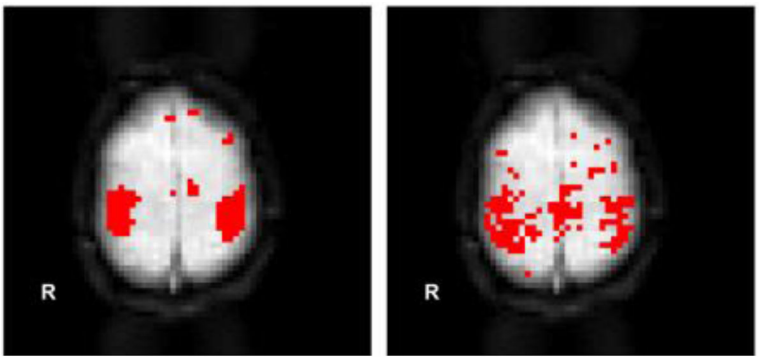

Figure 2.

(LEFT) Localization aid for primary motor cortex regions as revealed by a motor-stimulation task fMRI experiment. (RIGHT) Motor cortex regions recovered using our MCA framework. Dice coefficient achieved between the localization aid and our MCA network analysis results is 0.45.

Table 1

Results on the 50 synthetic models for different training time series lengths

Length of time series used for training	AUC (mean ± std)	Rand Index (mean ± std)
100	0.71 ± 0.041	0.75 ± 0.039
200	0.77 ± 0.051	0.76 ± 0.049
400	0.84 ± 0.046	0.82 ± 0.058
600	0.88 ± 0.045	0.85 ± 0.058
800	0.91 ± 0.038	0.86 ± 0.064
1000	0.92 ± 0.037	0.87 ± 0.063